Int J. Solids Structures Vol. 22, No 9, pp 1033–1053, 1986
Printed in Great Britain.

0020-7683/86 $3.00+ 00
Pergamon Journals Ltd

SMOOTH INDENTATION OF A TRANSVERSELY ISOTROPIC CANTILEVER BEAM

LEON M. KEER and WILLIAM P. SCHONBERG
Department of Civil Engineering, Northwestern University, Evanston, IL 60201, U.S.A.

(*Received* 19 *July* 1984; *in revised form* 23 *May* 1985)

Abstract—The response of a transversely isotropic beam of finite length to a frictionless cylindrical and flat indenter is studied. Solutions are obtained through a global–local technique, which accounts for the local behavior near the indenter, as well as the global beam behavior. The method of analysis superposes an infinite elastic layer solution derived through the use of integral transforms with a beam theory solution. Local indenter stresses, as well as displacements and rotations, are computed for each case and plotted for various ratios of contact width to beam length and for various positions of the indenters. To study the effects of anisotropy, each problem is solved using two materials: one nearly isotropic, the other highly anisotropic. Results are compared to those of an earlier isotropic study, and to Hertz theory and beam theory solutions.

1. INTRODUCTION

The study performed in this article continues the investigation of Keer and Schonberg[1] on isotropic cantilever beams. Consider now a finite, transversely isotropic layer, fixed on one end, free on the other, and loaded by an indenter that is cylindrical [Fig. 1(a)] or flat [Fig. 1(b)]. This problem is seen often in mechanical applications and may later also serve as a model for impact phenomena in turbine blades that are made of composite materials. Usual methods of solution are applicable only in a limited class of such problems. The method of solution used here is one that superposes an elastic layer solution with a Euler–Bernoulli beam theory solution. Layer solution loads at the ends of the beam are cancelled

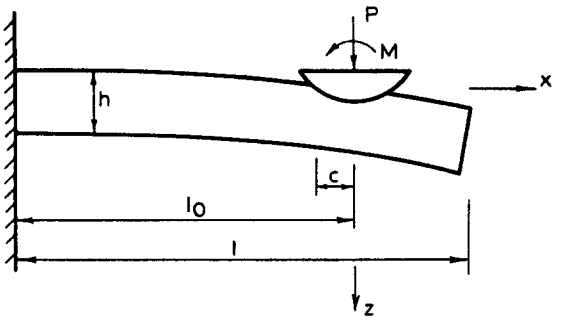

Fig. 1(a). Problem configuration (Case I).

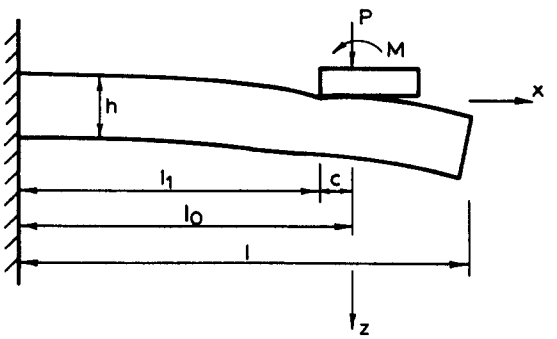

Fig. 1(b). Problem configuration (Case II).

by beam theory solution loads in such a manner that the boundary conditions there are satisfied. While the layer solution is an exact solution, it should be noted that for the case of a cantilever beam, a beam theory solution may or may not meet the requirements of compatibility, depending on the type of loading that is prescribed. Thus, in the superposition of a layer solution with a beam theory solution, there exists the possibility that two solutions having different orders of accuracy are being combined. A check of the compatibility of cantilever beam solutions indicates that concentrated end-load solutions (i.e. solutions in which the displacement functions are third degree polynomials) are exact. Therefore, the transverse displacement function of the beam theory solution is chosen to be a third degree polynomial. The resulting full solution is then a superposition of two exact solutions (beam theory plus elastic layer), where the coefficients in the displacement function are determined from the boundary conditions of a cantilever beam applied to appropriate full solution expressions. In this way the loading on the cantilever is dealt with by the layer solution, while the beam theory solution is responsible for the end conditions. In the enforcement of these conditions, it is assumed that thickness effects are negligible at the ends of the cantilever.

The physical quantities of interest are the stress distributions under each indenter and the displacements and rotations of the beams under each indenter. Following the procedure of Keer and Schonberg, an extensive study of the response of transversely isotropic cantilever beams subjected to various loading conditions is performed. The reader is referred to the earlier study involving cantilever beams for a more detailed description of the techniques used here.

The results of this study are compared to those for isotropic cantilever beams. To assess the effect of the transverse isotropy, each problem is solved for two materials: magnesium (nearly isotropic) and cadmium (highly orthotropic). The results are further compared to elementary beam theory solutions and Hertz theory solutions for accuracy assessments.

2. CASE I. CYLINDRICAL INDENTER—PROBLEM FORMULATION

The problem to be solved is that of an elastic layer of thickness h and length l that is transversely isotropic about the z axis and is indented by a cylindrical punch on its upper surface [Fig. 1(a)]. The conditions at the ends of the layer are those of a cantilever beam: clamped on the left and free on the right. The boundary conditions for the elastic layer problem and beam theory problem are, respectively, as follows.

Elastic layer (boundary conditions on $z = 0, h$):

$$\tau_{zz}(x,h) = 0, \qquad |x| < \infty, \tag{2.1}$$

$$\tau_{xz}(x,h) = 0, \qquad |x| < \infty, \tag{2.2}$$

$$\tau_{xz}(x,0) = 0, \qquad |x| < \infty, \tag{2.3}$$

$$\tau_{zz}(x,0) = 0, \qquad c < |x| < \infty, \tag{2.4}$$

$$u_z(x,0) = \Delta - x^2/2R, \qquad 0 < |x| < c. \tag{2.5}$$

Beam theory (boundary conditions at $x = -l_0, l-l_0$):

$$u_z = 0, \qquad x = -l_0, \tag{2.6}$$

$$\theta = 0, \qquad x = -l_0, \tag{2.7}$$

$$M = 0, \qquad x = l-l_0, \tag{2.8}$$

$$V = 0, \qquad x = l-l_0. \tag{2.9}$$

The superposition solution (layer plus beam theory) must satisfy eqns (2.1)–(2.9). A suitable elasticity solution that represents loading on the upper surface of such a layer and no loading on the lower surface can be obtained using the techniques of Sneddon[2] and Green and Zerna[3], and is found to be

$$\tau_{zz} = \int_0^\infty \frac{E_S(\xi)\cos\xi x + E_A(\xi)\sin\xi x}{D(\xi)} \times \{\sqrt{\nu_1}I(\xi)\cosh(\xi z/\sqrt{\nu_1}) + \sqrt{\nu_2}H(\xi)\cosh(\xi z/\sqrt{\nu_2}) - G(\xi)[\sqrt{\nu_1}\sinh(\xi z/\sqrt{\nu_1}) - \sqrt{\nu_2}\sinh(\xi z/\sqrt{\nu_2})]\}\,d\xi, \quad (2.10)$$

$$\tau_{xz} = -\int_0^\infty \frac{E_S(\xi)\sin\xi x - E_A(\xi)\cos\xi x}{D(\xi)} \times \{I(\xi)\sinh(\xi z/\sqrt{\nu_1}) + H(\xi)\sinh(\xi z/\sqrt{\nu_2}) - G(\xi)[\cosh(\xi z/\sqrt{\nu_1}) - \cosh(\xi z/\sqrt{\nu_2})]\}\,d\xi, \quad (2.11)$$

$$\tau_{xx} = \int_0^\infty \frac{E_S(\xi)\cos\xi x + E_A(\xi)\sin\xi x}{D(\xi)} \times \left\{-\frac{1}{\sqrt{\nu_1}}I(\xi)\cosh(\xi z/\sqrt{\nu_1}) - \frac{1}{\sqrt{\nu_2}}H(\xi)\cosh(\xi z/\sqrt{\nu_2}) + G(\xi)\left[\frac{1}{\sqrt{\nu_1}}\sinh(\xi z/\sqrt{\nu_1}) - \frac{1}{\sqrt{\nu_2}}\sinh(\xi z/\sqrt{\nu_2})\right]\right\}d\xi, \quad (2.12)$$

$$u_z = \frac{1}{c_{44}}\int_0^\infty \frac{E_S(\xi)\cos\xi x + E_A(\xi)\sin\xi x}{\xi D(\xi)} \times \left\{\frac{\kappa_1}{1+\kappa_1}I(\xi)\sinh(\xi z/\sqrt{\nu_1}) + \frac{\kappa_2}{1+\kappa_2}H(\xi)\sinh(\xi z/\sqrt{\nu_2}) - G(\xi)\left[\frac{\kappa_1}{1+\kappa_1}\cosh(\xi z/\sqrt{\nu_1}) - \frac{\kappa_2}{1+\kappa_2}\cosh(\xi z/\sqrt{\nu_2})\right]\right\}d\xi, \quad (2.13)$$

$$u_x = -\frac{1}{c_{44}}\int_0^\infty \frac{E_S(\xi)\sin\xi x - E_A(\xi)\cos\xi x}{\xi D(\xi)} \times \left\{\frac{\sqrt{\nu_1}}{1+\kappa_1}I(\xi)\cosh(\xi z/\sqrt{\nu_1}) + \frac{\sqrt{\nu_2}}{1+\kappa_2}H(\xi)\cosh(\xi z/\sqrt{\nu_2}) - G(\xi)\left[\frac{\sqrt{\nu_1}}{1+\kappa_1}\sinh(\xi z/\sqrt{\nu_1}) - \frac{\sqrt{\nu_2}}{1+\kappa_2}\sinh(\xi z/\sqrt{\nu_2})\right]\right\}d\xi, \quad (2.14)$$

where

$$D(\xi) = 2\sqrt{\nu_2}(ch\beta_1 ch\beta_2 - 1) - \frac{\nu_1+\nu_2}{\sqrt{\nu_1}}sh\beta_1 sh\beta_2, \quad (2.15)$$

$$G(\xi) = \sqrt{\left(\frac{\nu_2}{\nu_1}\right)}ch\beta_2 sh\beta_1 - ch\beta_1 sh\beta_2, \quad (2.16)$$

$$H(\xi) = ch\beta_1 ch\beta_2 - \sqrt{\left(\frac{\nu_2}{\nu_1}\right)} sh\beta_1 sh\beta_2 - 1, \tag{2.17}$$

$$I(\xi) = \sqrt{\left(\frac{\nu_2}{\nu_1}\right)} ch\beta_1 ch\beta_2 - sh\beta_1 sh\beta_2 - \sqrt{\left(\frac{\nu_2}{\nu_1}\right)}, \tag{2.18}$$

and $\beta_i = \xi h/\nu_i$. The material constants ν_i and κ_i are obtained using the technique outlined in Green and Zerna. The ν_i are the roots of the equation

$$K_{44}K_{11}\nu^2 - (K_{11}K_{33} - K_{13}^2 - 2K_{13}K_{44})\nu + K_{44}K_{33} = 0. \tag{2.19}$$

The κ_i are then obtained from the ν_i via the relationship

$$\kappa_i = \frac{K_{11}\nu_i - K_{44}}{K_{13} + K_{44}}, \tag{2.20}$$

where the K_{ij} are constant functions of the layer moduli c_{ij} and whether the layer is in a state of plane strain or plane stress. If a state of plane strain is assumed, then $K_{ij} = c_{ij}$; if plane stress is assumed, then $K_{11} = c_{11} - c_{12}^2/c_{11}$, $K_{13} = c_{13} - c_{12}c_{13}/c_{11}$, $K_{33} = c_{33} - c_{13}^2/c_{11}$ and $K_{44} = c_{44}$.

It is seen that on $y = h$, the normal and shear stresses vanish automatically, and that on $y = 0$, the shear stresses vanish. The normal stress on $y = 0$ is given as

$$\tau_{zz}(x, 0) = \int_0^\infty [E_S(\xi)\cos(\xi x) + E_A(\xi)\sin(\xi x)]\,d\xi. \tag{2.21}$$

Substituting

$$E_S(\xi) = \int_0^c \psi(t) J_0(\xi t)\,dt, \tag{2.22}$$

$$E_A(\xi) = \int_0^c \phi(t) J_1(\xi t)\,dt \tag{2.23}$$

into eqn (2.18) yields

$$\tau_{zz}(x, 0) = \int_x^c \frac{\psi(t)\,dt}{\sqrt{(t^2 - x^2)}} + x\int_x^c \frac{\phi(t)\,dt}{t\sqrt{(t^2 - x^2)}}. \tag{2.24}$$

The moment, shear and average slope due to the stresses as given by eqns (2.10)–(2.12) are given by

$$M_E = \int_0^h z\tau_{xx}\,dz = -\int_0^\infty \xi^{-2}[E_S(\xi)\cos\xi x + E_A(\xi)\sin\xi x]\,d\xi, \tag{2.25}$$

$$V_E = \int_0^h \tau_{xz}\,dz = \int_0^\infty \xi^{-1}[E_S(\xi)\sin\xi x - E_A(\xi)\cos\xi x]\,d\xi, \tag{2.26}$$

$$\bar{\theta}_E = \frac{1}{h}\int_0^h \frac{\partial u_z}{\partial x}\,dz = \frac{\sqrt{\nu_2}}{hc_{44}}\int_0^\infty \frac{F(\xi)}{D(\xi)}\xi^{-1}[E_S(\xi)\sin\xi x - E_A(\xi)\cos\xi x]\,d\xi, \tag{2.27}$$

where

$$F(\xi)=\left(\frac{\kappa_1}{1+\kappa_1}+\frac{\kappa_2}{1+\kappa_2}\right)(ch\beta_1 ch\beta_2-1)-\left(\frac{\kappa_1}{1+\kappa_1}\sqrt{\left(\frac{\nu_1}{\nu_2}\right)}+\frac{\kappa_2}{1+\kappa_2}\sqrt{\left(\frac{\nu_1}{\nu_2}\right)}\right)sh\beta_1 sh\beta_2$$
$$+\left(\frac{\kappa_1}{1+\kappa_1}-\frac{\kappa_2}{1+\kappa_2}\right)(ch\beta_1-ch\beta_2). \quad (2.28)$$

For the beam theory solution, the transverse displacement is taken to be of the form

$$u_z^B(x)=a_0+a_1x+a_2x^2+a_3x^3. \quad (2.29)$$

Assuming the hypotheses of Euler–Bernoulli beam theory, the following expressions for the moment, shear and average slope of a transversely isotropic beam are obtained:

$$M_B=-2D^*(a_2+3a_3x), \quad (2.30)$$

$$V_B=-6D^*a_3, \quad (2.31)$$

$$\bar{\theta}_B=a_1+2a_2x+3a_3x^2, \quad (2.32)$$

where the bending stiffness D^* is given by

$$D^*=\frac{h^3}{12}\left(c_{11}-\frac{c_{13}^2}{c_{33}}\right)(1-n^2), \quad (2.33)$$

with $n=0$ for plane strain, and $n=(c_{12}-c_{13}^2/c_{33})/(c_{11}-c_{13}^2/c_{33})$ for plane stress. The constants a_1, a_2 and a_3 are obtained by superposing appropriate beam theory expressions with corresponding layer expressions and applying the beam theory boundary conditions, given by eqns (2.6)–(2.9). The resulting expressions are

$$a_1=\frac{\sqrt{\nu_2}}{hc_{44}}\int_0^\infty\frac{F(\xi)}{D(\xi)}[E_S(\xi)\sin\xi l_0+E_A(\xi)\cos\xi l_0]\,d\xi$$
$$-\frac{1}{D^*}\int_0^\infty\left\{\frac{l_0(l-l_0/2)}{\xi}[E_S(\xi)\sin\xi(l-l_0)-E_A(\xi)\cos\xi(l-l_0)]\right.$$
$$\left.+\frac{l_0}{\xi^2}[E_S(\xi)\cos\xi(l-l_0)+E_A(\xi)\sin\xi(l-l_0)]\right\}d\xi, \quad (2.34)$$

$$a_2=-\frac{l-l_0}{2D^*}\int_0^\infty\xi^{-1}[E_S(\xi)\sin\xi(l-l_0)-E_A(\xi)\cos\xi(l-l_0)]\,d\xi$$
$$-\frac{1}{2D^*}\int_0^\infty\xi^{-2}[E_S(\xi)\cos\xi(l-l_0)+E_A(\xi)\sin\xi(l-l_0)]\,d\xi, \quad (2.35)$$

$$a_3=\frac{1}{6D^*}\int_0^\infty\xi^{-1}[E_S(\xi)\sin\xi(l-l_0)-E_A(\xi)\cos\xi(l-l_0)]\,d\xi. \quad (2.36)$$

Equation (2.5) is treated in a similar manner. Differentiating with respect to x, and separating the resulting equation into symmetric and antisymmetric components yields

$$\left.\frac{\partial u_z^E}{\partial x}(x,0)\right|_A+2a_2x=-\frac{x}{R}, \quad (2.37)$$

$$\frac{\partial u_z^L}{\partial x}(x,0)\bigg|_S + a_1 + 3a_3x^2 = 0. \tag{2.38}$$

Consider first eqn (2.37). Substituting for $u_z^E(x,0)$, combining terms in $E_S(\xi)$ and $E_A(\xi)$, and making use of eqns (2.22) and (2.23) yields

$$\int_0^c \psi(t)\int_0^\infty \left[\frac{D^*}{c_{44}}\left(\frac{\kappa_1}{1+\kappa_1}-\frac{\kappa_2}{1+\kappa_2}\right)\frac{G(\xi)}{D(\xi)}\sin\xi x - x\frac{\cos\xi(l-l_0)}{\xi^2} - x(l-l_0)\frac{\sin\xi(l-l_0)}{\xi}\right]J_0(\xi t)\,d\xi\,dt$$
$$+\int_0^c \phi(t)\int_0^\infty \left[x(l-l_0)\frac{\cos\xi(l-l_0)}{\xi} - x\frac{\sin\xi(l-l_0)}{\xi^2}\right]J_1(\xi t)\,d\xi\,dt = -\frac{D^*x}{R}. \tag{2.39}$$

The improper asymptotic behavior of the first term in the first kernel at infinity is adjusted by adding and subtracting the term

$$\frac{D^*}{c_{44}}\left(\frac{\kappa_1}{1+\kappa_1}-\frac{\kappa_2}{1+\kappa_2}\right)\frac{1}{\sqrt{v_1}-\sqrt{v_2}}\int_0^c \psi(t)\int_0^\infty \sin(\xi x)J_0(\xi t)\,d\xi\,dt.$$

After simplification, eqn (2.39) reduces to

$$\frac{D^*}{c_{44}}\left(\frac{\kappa_1}{1+\kappa_1}-\frac{\kappa_2}{1+\kappa_2}\right)\frac{1}{\sqrt{v_1}-\sqrt{v_2}}\psi(x)+\int_0^c \psi(t)K_1(x,t)\,dt-\int_0^c \phi(t)K_2(x,t)\,dt = -\frac{D^*x}{R}, \tag{2.40}$$

where

$$K_1(x,t) = \int_0^\infty \left\{\frac{D^*}{c_{44}}\left(\frac{\kappa_1}{1+\kappa_1}-\frac{\kappa_2}{1+\kappa_2}\right)\left[\frac{G(\xi)}{D(\xi)}-\frac{1}{\sqrt{v_1}-\sqrt{v_2}}\right]\xi x J_0(\xi x) - \frac{x}{\xi^2}\cos\xi(l-l_0)\right\}J_0(\xi t)\,d\xi - \frac{\pi}{2}x(l-l_0), \tag{2.41}$$

$$K_2(x,t) = (\pi/4)tx. \tag{2.42}$$

Returning to eqn (2.38), performing similar manipulations yields

$$\int_0^c \psi(t)\int_0^\infty \left[\frac{\sqrt{v_2}}{c_{44}}\frac{F(\xi)}{D(\xi)}\frac{\sin\xi l_0}{\xi} - \frac{l_0(l-l_0/2)}{D^*}\frac{\sin\xi(l-l_0)}{\xi} - \frac{l_0}{D^*}\frac{\cos\xi(l-l_0)}{\xi^2} + \frac{x^2}{D^*}\frac{\sin\xi(l-l_0)}{\xi}\right]$$
$$\times J_0(\xi t)\,d\xi\,dt + \int_0^c \phi(t)\int_0^\infty \left[-\frac{1}{c_{44}}\left(\frac{\kappa_1}{1+\kappa_1}-\frac{\kappa_2}{1+\kappa_2}\right)\frac{G(\xi)}{D(\xi)}\cos\xi x + \frac{\sqrt{v_2}}{c_{44}}\frac{F(\xi)}{D(\xi)}\frac{\cos\xi l_0}{\xi}\right.$$
$$\left. + \frac{l_0(l-l_0/2)}{D^*}\frac{\cos\xi(l-l_0)}{\xi} - \frac{l_0}{D^*}\frac{\sin\xi(l-l_0)}{\xi^2} - \frac{x^2}{2D^*}\frac{\cos\xi(l-l_0)}{\xi}\right]J_1(\xi t)\,d\xi\,dt = 0. \tag{2.43}$$

The improper asymptotic behavior of the first term in the second kernel is adjusted by adding and subtracting the term

$$-\frac{D^*}{c_{44}}\left(\frac{\kappa_1}{1+\kappa_1}-\frac{\kappa_2}{1+\kappa_2}\right)\frac{1}{\sqrt{v_1}-\sqrt{v_2}}\int_0^c \phi(t)\int_0^\infty \cos(\xi x)J_1(\xi t)\,d\xi\,dt.$$

After simplification, eqn (2.43) reduces to

$$\frac{D^*}{c_{44}}\left(\frac{\kappa_1}{1+\kappa_1}-\frac{\kappa_2}{1+\kappa_2}\right)\frac{1}{\sqrt{\nu_1}-\sqrt{\nu_2}}\phi(x)+\int_0^c \psi(t)K_3(x,t)\,dt+\int_0^c \phi(t)K_4(x,t)\,dt=0, \quad (2.44)$$

where

$$K_3(x,t)=(\pi/4)x^2, \quad (2.45)$$

$$K_4(x,t)=\int_0^\infty \frac{D^*}{c_{44}}\left(\frac{\kappa_1}{1+\kappa_1}-\frac{\kappa_2}{1+\kappa_2}\right)\left[\frac{G(\xi)}{D(\xi)}-\frac{1}{\sqrt{\nu_1}-\sqrt{\nu_2}}\right]\xi x J_1(\xi x)J_1(\xi t)\,d\xi. \quad (2.46)$$

Equations (2.40) and (2.44) are the two coupled integral equations for the unknown auxiliary functions $\psi(x)$, $\phi(x)$. Once $\psi(x)$, $\phi(x)$ are obtained, all necessary physical quantities may be calculated.

The normal stress under the indenter is calculated using eqn (2.24). The resultant load and moment due to the symmetric and antisymmetric components, respectively, of the normal stress are obtained as follows:

$$P=\int_{-c}^{c}\tau_{zz}\,dx=-\pi\int_0^c \psi(t)\,dt, \quad (2.47)$$

$$M=-\int_{-c}^{c}x\tau_{zz}\,dx=-\frac{\pi}{2}\int_0^c t\phi(t)\,dt. \quad (2.48)$$

The deflection under the indenter, Δ, is evaluated after first solving for the constant a_0 through the use of the boundary condition given by eqn (2.6):

$$a_0=\frac{1}{c_{44}}\left(\frac{\kappa_1}{1+\kappa_1}-\frac{\kappa_2}{1+\kappa_2}\right)\int_0^\infty \frac{G(\xi)}{D(\xi)}\xi^{-1}[E_S(\xi)\cos\xi l_0-E_A(\xi)\sin\xi l_0]\,d\xi+a_1 l_0-a_2 l_0^2+a_3 l_0^3. \quad (2.49)$$

After superposition of the two solutions, substitution and simplification, the final result is

$$\begin{aligned}\Delta=&\int_0^c\psi(t)\int_0^\infty\left[-\frac{1}{c_{44}}\left(\frac{\kappa_1}{1+\kappa_1}-\frac{\kappa_2}{1+\kappa_2}\right)\frac{G(\xi)}{D(\xi)}\frac{1-\cos\xi l_0}{\xi}+\frac{l_0\sqrt{\nu_2}}{hc_{44}}\frac{F(\xi)}{D(\xi)}\frac{\sin\xi l_0}{\xi}\right.\\&\left.-\frac{l_0^2}{2D^*}\frac{\cos\xi(l-l_0)}{\xi^2}-\frac{l_0^2(3l-l_0)}{6D^*}\frac{\sin\xi(l-l_0)}{\xi}\right]J_0(\xi t)\,d\xi\,dt\\&+\int_0^c\phi(t)\int_0^\infty\left[-\frac{1}{c_{44}}\left(\frac{\kappa_1}{1+\kappa_1}-\frac{\kappa_2}{1+\kappa_2}\right)\frac{G(\xi)}{D(\xi)}\frac{\sin\xi l_0}{\xi}+\frac{l_0\sqrt{\nu_2}}{hc_{44}}\frac{F(\xi)}{D(\xi)}\frac{\cos\xi l_0}{\xi}\right.\\&\left.-\frac{l_0^2}{2D^*}\frac{\sin\xi(l-l_0)}{\xi^2}+\frac{l_0^2(3l-l_0)}{6D^*}\frac{\cos\xi(l-l_0)}{\xi}\right]J_1(\xi t)\,d\xi\,dt.\end{aligned} \quad (2.50)$$

After adjusting the behavior of the kernels at infinity, further simplification yields

$$\Delta=\int_0^c\psi(t)K_5(t)\,dt+\int_0^c\phi(t)K_6(t)\,dt, \quad (2.51)$$

where

$$K_5(t) = \int_0^\infty \left\{ -\frac{1}{c_{44}}\left(\frac{\kappa_1}{1+\kappa_1} - \frac{\kappa_2}{1+\kappa_2}\right)\left[\frac{G(\xi)}{D(\xi)} - \frac{1}{\sqrt{\nu_1}-\sqrt{\nu_2}}\right]\frac{1-\cos\xi l_0}{\xi} \right.$$
$$+ \frac{l_0}{hc_{44}}\left[\sqrt{\nu_2}\frac{F(\xi)}{D(\xi)} - \left(\frac{\kappa_1\sqrt{\nu_1}}{1+\kappa_1} - \frac{\kappa_2\sqrt{\nu_2}}{1+\kappa_2}\right)\frac{1}{\sqrt{\nu_1}-\sqrt{\nu_2}}\right]\frac{\sin\xi l_0}{\xi}$$
$$\left. - \frac{l_0^2}{2D^*}\frac{\cos\xi(l-l_0)}{\xi^2}\right\} J_0(\xi t)\,\mathrm{d}\xi - \frac{\pi l_0^2(3l-l_0)}{12D^*}$$
$$- \frac{1}{c_{44}}\left(\frac{\kappa_1}{1+\kappa_2} - \frac{\kappa_2}{1+\kappa_2}\right)\frac{1}{\sqrt{\nu_1}-\sqrt{\nu_2}}\cosh^{-1}\left(\frac{l_0}{t}\right)$$
$$+ \frac{\pi l_0}{2hc_{44}}\left(\frac{\kappa_1\sqrt{\nu_1}}{1+\kappa_1} - \frac{\kappa_2\sqrt{\nu_2}}{1+\kappa_2}\right)\frac{1}{\sqrt{\nu_1}-\sqrt{\nu_2}}, \tag{2.52}$$

$$K_6(t) = \int_0^\infty \left\{ -\frac{1}{c_{44}}\left(\frac{\kappa_1}{1+\kappa_1} - \frac{\kappa_2}{1+\kappa_2}\right)\left[\frac{G(\xi)}{D(\xi)} - \frac{1}{\sqrt{\nu_1}-\sqrt{\nu_2}}\right]\frac{\sin\xi l_0}{\xi} \right.$$
$$\left. + \frac{l_0}{hc_{44}}\left[\sqrt{\nu_2}\frac{F(\xi)}{D(\xi)} - \left(\frac{\kappa_1\sqrt{\nu_1}}{1+\kappa_1} - \frac{\kappa_2\sqrt{\nu_2}}{1+\kappa_2}\right)\frac{1}{\sqrt{\nu_1}-\sqrt{\nu_2}}\right]\frac{\cos\xi l_0}{\xi}\right\} J_1(\xi t)\,\mathrm{d}\xi$$
$$- \frac{\pi l_0^2}{8D^*}t - \frac{1}{c_{44}}\left(\frac{\kappa_1}{1+\kappa_1} - \frac{\kappa_2}{1+\kappa_2}\right)\frac{1}{\sqrt{\nu_1}-\sqrt{\nu_2}}\frac{t}{l_0^2+\sqrt{(l_0^2-t^2)}}. \tag{2.53}$$

The rotation of the beam under the indenter is found by superposing eqns (2.27) and (2.32), and substituting for a_0, a_1, a_2 and a_3:

$$\bar{\theta}(x) = \int_0^c \psi(t)\int_0^\infty \left\{\frac{\sqrt{\nu_2}}{hc_{44}}\frac{F(\xi)}{D(\xi)}\left(\frac{\sin\xi x+\sin\xi l_0}{\xi}\right) - \frac{A(x)}{D^*}\frac{\sin\xi(l-l_0)}{\xi}\right.$$
$$\left. - \frac{l_0+x\cos\xi(l-l_0)}{D^*}\frac{}{\xi^2}\right\} J_0(\xi t)\,\mathrm{d}\xi\,\mathrm{d}t$$
$$+ \int_0^c \phi(t)\int_0^\infty \left\{-\frac{\sqrt{\nu_2}}{hc_{44}}\frac{F(\xi)}{D(\xi)}\left(\frac{\cos\xi x-\cos\xi l_0}{\xi}\right) + \frac{A(x)}{D^*}\frac{\cos\xi(l-l_0)}{\xi}\right.$$
$$\left. - \frac{l_0+x\sin\xi(l-l_0)}{D^*}\frac{}{\xi^2}\right\} J_1(\xi t)\,\mathrm{d}\xi\,\mathrm{d}t, \tag{2.54}$$

where

$$A(x) = l_0(l-l_0/2)+x(l-l_0)-x^2/2. \tag{2.55}$$

After adjusting the behavior of the kernels at infinity, further simplification yields:

$$\bar{\theta}(x) = \frac{1}{hc_{44}}\left(\frac{\kappa_1\sqrt{\nu_1}}{1+\kappa_1} - \frac{\kappa_2\sqrt{\nu_2}}{1+\kappa_2}\right)\mathrm{sgn}\,(x)\left\{H(c-|x|)\left[\frac{\pi}{2}\int_0^{|x|}\psi(t)\,\mathrm{d}t\right.\right.$$
$$\left. + \int_{|x|}^c \psi(t)\sin^{-1}\left(\frac{|x|}{t}\right)\mathrm{d}t\right] + H(|x|-c)\frac{\pi}{2}\int_0^c \psi(t)\,\mathrm{d}t\Bigg\}$$
$$+ \int_0^c \psi(t)K_7(t)\,\mathrm{d}t + \int_0^c \phi(t)\,K_8(t)\,\mathrm{d}t, \tag{2.56}$$

$$K_7(t) = \int_0^\infty \left\{ \frac{1}{hc_{44}} \left[\sqrt{\nu_2} \frac{F(\xi)}{D(\xi)} - \left(\frac{\kappa_1\sqrt{\nu_1}}{1+\kappa_1} - \frac{\kappa_2\sqrt{\nu_2}}{1+\kappa_2} \right) \frac{1}{\sqrt{\nu_1}-\sqrt{\nu_2}} \right] \frac{\sin \xi x + \sin \xi l_0}{\xi} \right.$$
$$\left. - \frac{l_0 + x\cos\xi(l-l_0)}{D^*} \frac{}{\xi^2} \right\} J_0(\xi t)\, d\xi - \frac{\pi A(x)}{2D^*} + \frac{\pi}{2hc_{44}} \left(\frac{\kappa_1\sqrt{\nu_1}}{1+\kappa_1} - \frac{\kappa_2\sqrt{\nu_2}}{1+\kappa_2} \right) \frac{1}{\sqrt{\nu_1}-\sqrt{\nu_2}}, \quad (2.57)$$

$$K_8(t) = \int_0^\infty \left\{ -\frac{1}{hc_{44}} \left[\sqrt{\nu_2} \frac{F(\xi)}{D(\xi)} - \left(\frac{\kappa_1\sqrt{\nu_1}}{1+\kappa_1} - \frac{\kappa_2\sqrt{\nu_2}}{1+\kappa_2} \right) \frac{1}{\sqrt{\nu_1}-\sqrt{\nu_2}} \right] \frac{\cos \xi x - \cos \xi l_0}{\xi} \right\}$$
$$\times J_1(\xi t)\, d\xi - \frac{\pi}{4} \frac{l_0 + x}{D^*} t. \quad (2.58)$$

The rotation of the beam is calculated at the point under the indenter about which the moment produced by the antisymmetric stresses is zero. This point is obtained from statics simply as $x = -e = M/P$.

3. PROBLEM SOLUTION

The auxiliary functions $\psi(x)$ and $\phi(x)$ are obtained by solving equations (2.40) and (2.44) numerically. These equations are nondimensionalized through the use of the following parameters:

$$\delta = c/h, \qquad \varepsilon = e/h, \quad (3.1a,b)$$
$$\alpha = l_0/h, \qquad \gamma = l/h, \quad (3.1c,d)$$
$$u = t/c, \qquad y = x/c, \quad (3.1e,f)$$

$$\psi(x) = \left[\frac{1}{c_{44}} \left(\frac{\kappa_1}{1+\kappa_1} - \frac{\kappa_2}{1+\kappa_2} \right) \right]^{-1} \frac{cy}{R} \Psi(y), \quad (3.2)$$

$$\phi(x) = \left[\frac{1}{c_{44}} \left(\frac{\kappa_1}{1+\kappa_1} - \frac{\kappa_2}{1+\kappa_2} \right) \right]^{-1} \frac{cy}{R} \Phi(y). \quad (3.3)$$

Conditions of plane strain are assumed for the solution of eqns (2.40) and (2.44) and for the evaluation of the constants ν_i, κ_i and D^*. In this manner, we are also given an insight into the response of a long rectangular plate that is subjected to cylindrical indentation. Once the nondimensionalized auxiliary functions $\Psi(y)$, $\Phi(y)$ are obtained, eqns (2.24), (2.47), (2.48), (2.51) and (2.56) are used to calculate nondimensionalized stress, loads moments, deflections and rotations. These nondimensionalized quantities are transformed back to real quantities via the following relationships:

$$\tau_{zz} = P\hat{\tau}_{zz}/c, \quad (3.4)$$

$$P = \left[\frac{1}{c_{44}} \left(\frac{\kappa_1}{1+\kappa_1} - \frac{\kappa_2}{1+\kappa_2} \right) \right]^{-1} \hat{P}h^2/R, \quad (3.5)$$

$$M = \left[\frac{1}{c_{44}} \left(\frac{\kappa_1}{1+\kappa_1} - \frac{\kappa_2}{1+\kappa_2} \right) \right]^{-1} \hat{M}h^3/R, \quad (3.6)$$

$$\Delta = h^2\hat{\Delta}/R, \quad (3.7)$$

$$\bar{\theta} = h\hat{\bar{\theta}}/R. \quad (3.8)$$

The results of this study are checked in two ways. First, the symmetric component of the normal stress under the indenter is compared to a Hertzian contact stress solution. The Hertz solution is found by letting $c/h \to 0$ in eqns (2.40) and (2.44). In this case, the auxiliary functions are given by

$$\psi_H(x) = -(\sqrt{\nu_1}-\sqrt{\nu_2})x\left[\frac{R}{c_{44}}\left(\frac{\kappa_1}{1+\kappa_1}-\frac{\kappa_2}{1+\kappa_2}\right)\right]^{-1}, \tag{3.9}$$

$$\phi_H(x) = 0. \tag{3.10}$$

Substituting eqns (3.9) and (3.10) into eqn (2.24) and integrating yields

$$\tau_{zz}^{\text{Hertz}} = -(\sqrt{\nu_1}-\sqrt{\nu_2})\sqrt{(c^2-x^2)}\left[\frac{R}{c_{44}}\left(\frac{\kappa_1}{1+\kappa_1}-\frac{\kappa_2}{1+\kappa_2}\right)\right]^{-1}. \tag{3.11}$$

Second, the displacement and rotation of the beam under the indenter are compared with the corresponding values derived from the following classical transversely isotropic beam theory expressions:

$$\Delta_{BT} = (2Pl_0^3+3Ml_0^2)/6D^*, \tag{3.12}$$

$$\bar{\theta}_{BT} = [P(l_0^2-e^2)+2M(l_0-e)]/2D^*, \tag{3.13}$$

where P and M are the load and moment as calculated by eqns (2.47) and (2.48), respectively.

If an experimental verification of the results is desired, then conditions of plane stress must be assumed in the solution of eqns (2.40) and (2.44). This assumption would be consistent with the use of a thin beam in a laboratory study. A check of the constants appearing in eqns (2.40), (2.44), (2.51) and (2.56) reveals that the response of a beam made of a highly anisotropic material, such as cadmium, is very sensitive to whether the beam is assumed to be in a state of plane strain or plane stress. Thus, in an experimental study, one must be very careful to make sure that the experimental setup accurately models the assumed state of stress.

4. OBSERVATIONS AND CONCLUSIONS

Two transversely isotropic materials were chosen for this study. The first, magnesium, is nearly isotropic. To study the effect of more severe anisotropy, the second material was chosen to be cadmium. The elastic moduli of the two materials are listed in Table 1. For each material, solutions were obtained for $l/h = 10.0$ and 20.0, and for each l/h, $l_0/h = 0.25l/h$, $0.5l/h$ and $0.75l/h$. It was found that for small values of c/h the stress distributions for different values of l/h remained virtually identical. However, for larger values of c/h (i.e. $c/h > 0.5$), the stress distributions began to differ. This behavior is illustrated in Table 2, which compares peak total stresses for different values of c/h and l_0/h for a beam with $l/h = 10$. It was found that the peak total stresses in cadmium beams were generally less than those in magnesium beams. By comparison with the data obtained for steel beams[1],

Table 1. Elastic moduli for magnesium and cadmium (in N m^{-2})

	Magnesium	Cadmium
c_{11}	5.857×10^{10}	10.920×10^{10}
c_{12}	2.501×10^{10}	3.976×10^{10}
c_{13}	2.079×10^{10}	3.754×10^{10}
c_{33}	6.110×10^{10}	4.602×10^{10}
c_{44}	1.658×10^{10}	1.562×10^{10}

Table 2. Peak total stresses (Case 1, $l/h = 10.0$)

	Cadmium			Magnesium		
c/h	$l_0/h = 2.5$	$l_0/h = 5.0$	$l_0/h = 7.5$	$l_0/h = 2.5$	$l_0/h = 5.0$	$l_0/h = 7.5$
0.1	0.6361	0.6361	0.6361	0.6361	0.6361	0.6361
0.2	0.6333	0.6362	0.6362	0.6362	0.6295	0.6362
0.5	0.6360	0.6399	0.6382	0.6707	0.6560	0.6493
0.8	0.7057	0.6986	0.6968	—	—	0.7911

it was found that the peak total stresses in magnesium beams were less than those in steel beams. Therefore, it can be concluded that in the case of cylindrical indentation, the general effect of increased anisotropy is to lower the total normal stress under the indenter. It is noted that the resultant changes in peak total stress are on the order of 2% for small contact lengths, but can go as high as 20% (magnesium) or 30% (cadmium) for large contact lengths.

A typical symmetric stress distribution is shown in Fig. 2; that of the total stress under the indenter is shown in Fig. 3. As can be seen in Fig. 2, for small values of c/h the Hertzian distribution approximates the stress under the indenter quite well. As c/h increases, the effect of the antisymmetric nature of the problem increases, and the distribution changes significantly. In Fig. 3, this effect is seen as the location of the peak total stress shifts to the left and the distribution becomes less and less parabolic. Tables 3 and 4 show a comparison between the elasticity solutions developed here and the classical beam theory solutions. The elasticity solutions for both material types are seen to agree well with the beam theory solutions.

Upon examination of the load vs contact length and load vs displacement data, it was found that for the same load, cadmium beams experienced a larger contact length than the corresponding magnesium beams. Or, for the same contact length, magnesium beams can tolerate a higher load than cadmium beams. This is illustrated in Fig. 4 for the case where $l/h = 10.0$. Similarly, it was found that for the same load, the magnesium beams experienced a larger deflection under the indenter than the cadmium beams, as is illustrated in Fig. 5 for the case where $l/h = 20.0$. In Fig. 5, the nondimensionalized load parameter defined in eqn (3.5) was rewritten as

$$\hat{P} = \lambda(c_{ij})hPR/D^*, \tag{4.1}$$

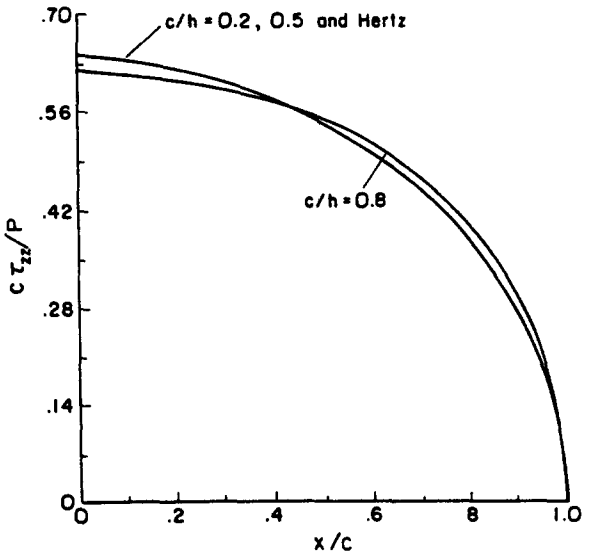

Fig. 2. Symmetric stress distribution (Case I) (magnesium; $l/h = 20.0$, $l_0/h = 15.0$).

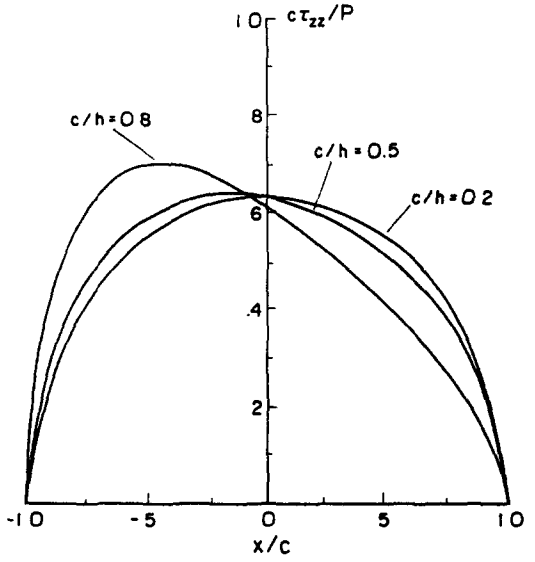

Fig. 3 Total stress distribution (Case I) (magnesium; $l/h = 20.0$, $l_0/h = 15.0$).

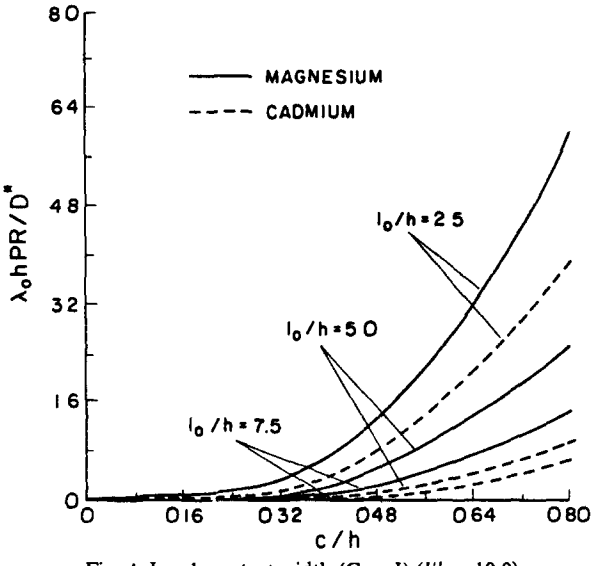

Fig 4. Load–contact width (Case I) ($l/h = 10.0$).

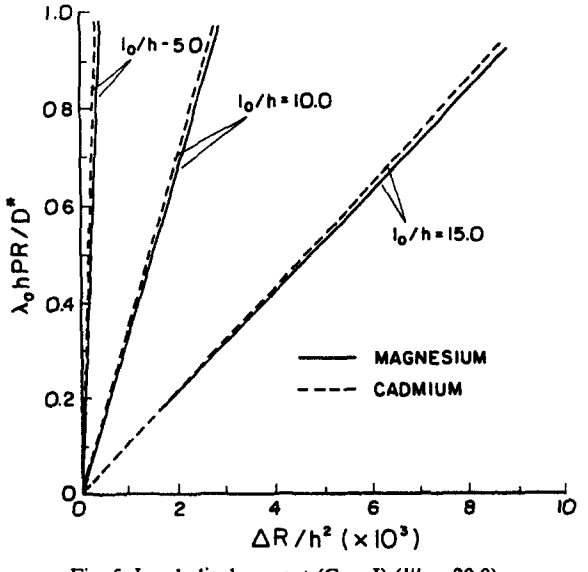

Fig 5. Load–displacement (Case I) ($l/h = 20.0$).

Table 3. Displacement comparison (Case I)

		$l_0/h = 2.5$		$l_0/h = 5.0$		$l_0/h = 7.5$		
		Elasticity	Beam theory	Elasticity	Beam theory	Elasticity	Beam theory	c/h
Cadmium	$l/h = 10.0$	0.25	0.25	2.02	2.02	6.78	6.78	0.1
		1.04	1.04	8.29	8.30	27.36	27.38	0.2
		5.08	5.09	37.28	37.37	115.26	115.41	0.4
		156.35	159.59	291.89	293.20	658.92	660.20	0.8
Magnesium	$l/h = 10.0$	0.48	0.48	3.86	3.86	13.00	13.00	0.1
		2.01	2.01	16.15	16.15	52.86	52.87	0.2
		12.63	12.67	83.94	84.04	232.31	232.46	0.4
		—	—	—	—	1646.09	1647.74	0.8

where $\lambda(c_{ij})$ is a function of the elastic constants of each material. It was found that the values of $\lambda(c_{ij})$ for cadmium and magnesium were virtually identical. Thus, defining λ_0 as the average of the two values, eqn (4.1) can be rewritten as

$$\hat{P} = \lambda_0 hPR/D^*. \tag{4.2}$$

Through such a representation of the load parameter, the effect of the difference in bending stiffness between the two beam types is seen more clearly. The behavior illustrated in Fig. 5 is due to the combined effect of lower and higher stiffnesses in the vertical and horizontal directions, respectively, of the cadmium beams. As such, the bending stiffness of a cadmium beam is greater than the bending stiffness of a magnesium beam. As the load increases, in the case of the transversely softer cadmium beams, the indenter penetrates more deeply into the beam. This results in a larger contact length (e.g. Fig. 4), as well as in a smaller deflection (e.g., Fig. 5).

It is interesting to note that in this study, as well as in the one performed on isotropic beams[1], although the local–global formulation used rendered the problems nonlinear, the load–displacement curves were, in the regions indicated, virtually linear. This characteristic is drastically different from that of the load–displacement curves obtained by Miller[4] and Ballarini[5], which are highly nonlinear in nature. Such differences in behavior are due to the effect of wrapping being negligible in the case of a cantilever beam. If the beam is either simply supported or clamped on both sides,the effect of wrapping is much more pronounced. For the range of loads and displacements considered here, the nonlinearities introduced by wrapping are hardly noticeable.

To ensure that the actual rotations are "small", the following lower bound must be placed on R/h:

$$R/h > \hat{\theta}/\bar{\theta}_0. \tag{4.3}$$

Table 4. Rotation comparison (Case I)

		$l_0/h = 2.5$		$l_0/h = 5.0$		$l_0/h = 7.5$		
		Elasticity	Beam theory	Elasticity	Beam theory	Elasticity	Beam theory	c/h
Cadmium	$l/h = 10.0$	0.14	0.15	0.60	0.61	1.34	1.36	0.1
		0.58	0.62	2.45	2.49	5.44	5.48	0.2
		2.86	3.05	11.03	11.20	22.91	23.07	0.4
		88.97	93.07	86.00	86.89	130.43	131.02	0.8
Magnesium	$l/h = 10.0$	0.28	0.29	1.14	1.16	2.59	2.60	0.1
		1.15	1.20	4.79	4.84	10.52	10.58	0.2
		7.27	7.58	24.93	25.18	46.24	46.45	0.4
		—	—	—	—	324.94	325.13	0.8

Table 5 Minimum allowable values of R/h (Case I).

		$l/h = 10.0$			$l/h = 20.0$		
	c/h	$l_0/h = 2.5$	$l_0/h = 5.0$	$l_0/h = 7.5$	$l_0/h = 5.0$	$l_0/h = 10.0$	$l_0/h = 15.0$
Cadmium	0.1	0.5	1.8	3.9	1.8	6.9	15.7
	0.2	1.8	7.0	15.6	7 3	28.4	64.1
	0.4	8.2	31 6	66.1	36.0	147.2	289.0
	0.8	278.5	246.5	373.8	—	—	2306 5
Magnesium	0.1	0.8	3 3	7.5	3.4	13.3	29 8
	0.2	3.3	13.8	30.2	14.9	60.5	124.9
	0.4	20.9	71.5	132.5	127.9	577.1	651.0
	0.8	—	—	929.4	—	—	55,801.5

Assuming the value $\bar{\theta}_0 = 20°$ (0.349 rad), Table 5 shows the minimum allowable values of R/h to ensure small deflections and no yielding.

The results discussed here demonstrate clearly that transversely isotropic materials, having a preferred direction, are very sensitive to loadings in their non-preferred directions. These results can be further used to estimate the behavior of compositie materials, since they also exhibit this kind of behavior.

5. CASE II: FLAT INDENTER—PROBLEM FORMULATION

The problem to be solved is that of an elastic, transversely isotropic layer of thickness h and length l indented by a flat punch on its upper surface [Fig. 1(b)]. The boundary conditions for the elasticity problem and beam theory problem whose solutions shall be superposed to form the full solution are, respectively, as follows.

Elastic layer (boundary conditions on $z = 0, h$):

$$\tau_{zz}(x, h) = 0, \qquad |x| < \infty, \tag{5.1}$$

$$\tau_{xz}(x, h) = 0, \qquad |x| < \infty, \tag{5.2}$$

$$\tau_{xz}(x, 0) = 0, \qquad |x| < \infty, \tag{5.3}$$

$$\tau_{zz}(x, 0) = 0, \qquad c < |x| < \infty, \tag{5.4}$$

$$u_z(x, 0) = \Delta, \qquad 0 < |x| < c. \tag{5.5}$$

Beam theory (boundary conditions at $x = -l_0, l-l_0$):

$$u_z = 0, \qquad x = -l_0, \tag{5.6}$$

$$\bar{\theta} = 0, \qquad x = -l_0, \tag{5.7}$$

$$M = 0, \qquad x = l-l_0, \tag{5.8}$$

$$V = 0, \qquad x = l-l_0. \tag{5.9}$$

It is further required that the normal stress be nonsingular at $x = c$:

$$|\tau_{zz}(c, 0)| < \infty. \tag{5.10}$$

This condition ensures a smooth deflection of the beam for $x > 0$ and results in a decreasing contact length with increase of load.

The suitable elasticity solution for this problem is given by eqns (2.10) through (2.15). Using this formulation, the normal stress is given by

$$\tau_{zz} = \int_0^\infty [E_S(\xi)\cos\xi x + E_A(\xi)\sin\xi x]\,d\xi. \tag{5.11}$$

For a flat punch, we let

$$E_S(\xi) = AJ_0(\xi c) + \int_0^c \psi(t)J_0(\xi t)\,d\xi, \tag{5.12}$$

$$E_A(\xi) = BJ_1(\xi c) + \int_0^c \phi(t)J_1(\xi t)\,d\xi. \tag{5.13}$$

Substituting into eqn (5.11), it becomes evident that the singularity at $x = c$ disappears if $A = -B$. Making use of this substitution, eqn (5.11) becomes

$$\tau_{zz}(x,0) = -\frac{B}{c}\frac{c-x}{\sqrt{(c^2-x^2)}}H(c-x) + \int_0^c \frac{\psi(t)\,dt}{\sqrt{(t^2-x^2)}} + x\int_x^c \frac{\phi(t)\,dt}{t\sqrt{(t^2-x^2)}}. \tag{5.14}$$

The moment, shear and average slope are given by eqns (2.25), (2.26) and (2.27), respectively. As before, the beam theory solution is taken to be

$$u_z^B(x) = a_0 + a_1x + a_2x^2 + a_3x^3, \tag{5.15}$$

resulting in expressions for moment, shear and average slope given by eqns (2.30), (2.31) and (2.32), respectively. The constants a_1, a_2 and a_3 are obtained as before, with identical outcome. Differentiating eqn (5.5) with respect to x, and separating the resulting equation into symmetric and antisymmetric component yields

$$\left.\frac{\partial u_z^E}{\partial x}(x,0)\right|_A + 2a_2x = 0, \tag{5.16}$$

$$\left.\frac{\partial u_z^E}{\partial x}(x,0)\right|_S + a_1 + 3a_3x^2 = 0. \tag{5.17}$$

Considering each equation one at a time and following the same procedure as before results in the following equations for A, B, $\psi(t)$ and $\phi(t)$:

$$AK_1(x,c) + \frac{D^*}{c_{44}}\left(\frac{\kappa_1}{1+\kappa_1} - \frac{\kappa_2}{1+\kappa_2}\right)\frac{1}{\sqrt{\nu_1}-\sqrt{\nu_2}}\psi(x) + \int_0^c \psi(t)K_1(x,t)\,dt - BK_2(x,c) - \int_0^c \phi(t)K_2(x,t) = 0, \tag{5.18}$$

$$AK_3(x,c) + \int_0^c \psi(t)K_3(x,t)\,dt + BK_4(x,c) + \frac{D^*}{c_{44}}\left(\frac{\kappa_1}{1+\kappa_1} - \frac{\kappa_2}{1+\kappa_2}\right)\frac{1}{\sqrt{\nu_1}-\sqrt{\nu_2}}\phi(x) + \int_0^c \phi(t)K_4(x,t)\,dt = 0, \tag{5.19}$$

where

$$K_1(x,\eta)=\int_0^\infty\left\{\frac{D^*}{c_{44}}\left(\frac{\kappa_1}{1+\kappa_1}+\frac{\kappa_2}{1+\kappa_2}\right)\left[\frac{G(\xi)}{D(\xi)}-\frac{1}{\sqrt{\nu_1}-\sqrt{\nu_2}}\right]\xi x J_0(\xi x)\right.$$
$$\left.-\frac{x}{\xi^2}\cos\xi(l-l_0)\right\}J_0(\xi\eta)\,d\xi-\frac{\pi}{2}x(l-l_0), \quad (5.20)$$

$$K_2(x,\eta)=(\pi/4)x\eta, \quad (5.21)$$

$$K_3(x,\eta)=(\pi/4)x^2, \quad (5.22)$$

$$K_4(x,\eta)=\int_0^\infty\frac{D^*}{c_{44}}\left(\frac{\kappa_1}{1+\kappa_1}-\frac{\kappa_2}{1+\kappa_2}\right)\left[\frac{G(\xi)}{D(\xi)}-\frac{1}{\sqrt{\nu_1}-\sqrt{\nu_2}}\right]\xi x J_1(\xi x)J_1(\xi\eta)\,d\xi, \quad (5.23)$$

and $\eta = c$ or t. Equations (5.18) and (5.19) are two equations in four unknowns. A third equation was obtained earlier by eliminating the singularity of the normal stress at $x = c$ (i.e. $A+B=0$). The fourth equation is found by enforcing the boundary condition given by eqn (5.5). This yields the following expression for the constant B:

$$B=\left[\Delta-\int_0^c\psi(t)K_5(t)\,dt-\int_0^c\phi(t)K_6(t)\,dt\right]\Big/[K_6(c)-K_5(c)], \quad (5.24)$$

where

$$K_5(\eta)=\int_0^\infty\left\{-\frac{1}{c_{44}}\left(\frac{\kappa_1}{1+\kappa_2}-\frac{\kappa_2}{1+\kappa_2}\right)\left[\frac{G(\xi)}{D(\xi)}-\frac{1}{\sqrt{\nu_1}-\sqrt{\nu_2}}\right]\frac{1-\cos\xi l_0}{\xi}\right.$$
$$+\frac{l_0}{hc_{44}}\left[\sqrt{\nu_2}\frac{F(\xi)}{D(\xi)}-\left(\frac{\kappa_1\sqrt{\nu_1}}{1+\kappa_1}-\frac{\kappa_2\sqrt{\nu_2}}{1+\kappa_2}\right)\frac{1}{\sqrt{\nu_1}-\sqrt{\nu_2}}\right]\frac{\sin\xi l_0}{\xi}$$
$$\left.-\frac{l_0^2}{2D^*}\frac{\cos\xi(l-l_0)}{\xi^2}\right\}J_0(\xi\eta)\,d\xi-\frac{\pi l_0^2(3l-l_0)}{12D^*}$$
$$-\frac{1}{c_{44}}\left(\frac{\kappa_1}{1+\kappa_1}-\frac{\kappa_2}{1+\kappa_2}\right)\frac{1}{\sqrt{\nu_1}-\sqrt{\nu_2}}\cosh^{-1}\left(\frac{l_0}{\eta}\right)$$
$$+\frac{\pi l_0}{2hc_{44}}\left(\frac{\kappa_1\sqrt{\nu_1}}{1+\kappa_1}-\frac{\kappa_2\sqrt{\nu_2}}{1+\kappa_2}\right)\frac{1}{\sqrt{\nu_1}-\sqrt{\nu_2}}, \quad (5.25)$$

$$K_6(\eta)=\int_0^\infty\left\{-\frac{1}{c_{44}}\left(\frac{\kappa_1}{1+\kappa_1}-\frac{\kappa_2}{1+\kappa_2}\right)\left[\frac{G(\xi)}{D(\xi)}-\frac{1}{\sqrt{\nu_1}-\sqrt{\nu_2}}\right]\frac{\sin\xi l_0}{\xi}\right.$$
$$\left.+\frac{l_0}{hc_{44}}\left[\sqrt{\nu_2}\frac{F(\xi)}{D(\xi)}-\left(\frac{\kappa_1\sqrt{\nu_1}}{1+\kappa_1}-\frac{\kappa_2\sqrt{\nu_2}}{1+\kappa_2}\right)\frac{1}{\sqrt{\nu_1}-\sqrt{\nu_2}}\right]\frac{\cos\xi l_0}{\xi}\right\}J_1(\xi\eta)\,d\xi$$
$$-\frac{1}{c_{44}}\left(\frac{\kappa_1}{1+\kappa_1}-\frac{\kappa_2}{1+\kappa_2}\right)\frac{1}{\sqrt{\nu_1}-\sqrt{\nu_2}}\frac{\eta}{l_0+\sqrt{(l_0^2-\eta^2)}}-\frac{\pi l_0^2}{8D^*}\eta, \quad (5.26)$$

and $\eta = c$ or t. Making use of eqn (5.25) in eqns (5.18) and (5.19) yields

$$\frac{D^*}{c_{44}}\left(\frac{\kappa_1}{1+\kappa_1}-\frac{\kappa_2}{1+\kappa_2}\right)\frac{1}{\sqrt{\nu_1}-\sqrt{\nu_2}}\psi(x)+\int_0^c\psi(t)\left[K_1(x,t)-\frac{K_1(x,c)+K_2(x,c)}{K_5(c)-K_6(c)}K_5(t)\right]dt$$
$$-\int_0^c\phi(t)\left[K_2(x,t)+\frac{K_1(x,c)+K_2(x,c)}{K_5(c)-K_6(c)}K_6(t)\right]dt=-\Delta\frac{K_1(x,c)+K_2(x,c)}{K_5(c)-K_6(c)}, \quad (5.27)$$

$$\frac{D^*}{c_{44}}\left(\frac{\kappa_1}{1+\kappa_1}-\frac{\kappa_2}{1+\kappa_2}\right)\frac{1}{\sqrt{\nu_1}-\sqrt{\nu_2}}\phi(x)+\int_0^c\psi(t)\left[K_3(x,t)-\frac{K_3(x,c)-K_4(x,c)}{K_5(c)-K_6(c)}K_5(t)\right]dt$$
$$+\int_0^c\phi(t)\left[K_4(x,t)-\frac{K_3(x,c)-K_4(x,c)}{K_5(c)-K_6(c)}K_6(t)\right]dt=-\Delta\frac{K_3(x,c)-K_4(x,c)}{K_5(c)-K_6(c)}. \quad (5.28)$$

Equations (5.27) and (5.28) are solved numerically for the unknown auxiliary functions $\psi(x)$ and $\phi(x)$. Once $\psi(x)$ and $\phi(x)$ are obtained, all necessary physical quantities may then be calculated. The normal stress under the indenter is calculated using eqn (5.14). The resultant load and moment are given by

$$P=\pi B-\pi\int_0^c\psi(t)\,dt, \quad (5.29)$$

$$M=-\frac{\pi}{2}Bc-\frac{\pi}{2}\int_0^c t\phi(t)\,dt. \quad (5.30)$$

The rotation of the beam at any point $x>c$ is given by

$$\bar{\theta}(x)=B[K_8(x,c)-K_7(x,c)]+\int_0^c\psi(t)K_7(x,t)\,dt+\int_0^c\phi(t)K_8(x,t)\,dt$$
$$-\frac{\pi}{2hc_{44}}\left(\frac{\kappa_1\sqrt{\nu_1}}{1+\kappa_1}-\frac{\kappa_2\sqrt{\nu_2}}{1+\kappa_2}\right)\frac{1}{\sqrt{\nu_1}-\sqrt{\nu_2}}\left[B-\int_0^c\psi(t)\,dt\right], \quad (5.31)$$

where

$$K_7(x,\eta)=\int_0^\infty\left\{\frac{1}{hc_{44}}\left[\sqrt{\nu_2}\frac{F(\xi)}{D(\xi)}-\left(\frac{\kappa_1\sqrt{\nu_1}}{1+\kappa_1}-\frac{\kappa_2\sqrt{\nu_2}}{1+\kappa_2}\right)\frac{1}{\sqrt{\nu_1}-\sqrt{\nu_2}}\right]\frac{\sin\xi x+\sin\xi l_0}{\xi}\right.$$
$$\left.-\frac{l_0+x}{D^*}\frac{\cos\xi(l-l_0)}{\xi^2}\right\}J_0(\xi\eta)\,d\xi-\frac{\pi A(x)}{2D^*}+\frac{\pi}{2hc_{44}}\left(\frac{\kappa_1\sqrt{\nu_1}}{1+\kappa_1}-\frac{\kappa_2\sqrt{\nu_2}}{1+\kappa_2}\right)\frac{1}{\sqrt{\nu_1}-\sqrt{\nu_2}}, \quad (5.32)$$

$$K_8(x,t)=\int_0^\infty\left\{-\frac{1}{hc_{44}}\left[\sqrt{\nu_2}\frac{F(\xi)}{D(\xi)}-\left(\frac{\kappa_1\sqrt{\nu_1}}{1+\kappa_1}-\frac{\kappa_2\sqrt{\nu_2}}{1+\kappa_2}\right)\right.\right.$$
$$\left.\left.\times\frac{1}{\sqrt{\nu_1}-\sqrt{\nu_2}}\right]\frac{\cos\xi x-\cos\xi l_0}{\xi}\right\}J_1(\xi\eta)\,d\xi-\frac{\pi}{4}\frac{l_0+x}{D^*}\eta, \quad (5.33)$$

and $\eta=c$ or t.

6. PROBLEM SOLUTION

Following a scheme similar to that of Section 3, we define

$$\alpha_1=l_1/h, \quad (6.1)$$

$$\psi(x)=\left[\frac{1}{c_{44}}\left(\frac{\kappa_1}{1+\kappa_1}-\frac{\kappa_2}{1+\kappa_2}\right)\right]^{-1}\frac{\Delta cx}{h^2}\Psi(x), \quad (6.2)$$

$$\phi(x)=\left[\frac{1}{c_{44}}\left(\frac{\kappa_1}{1+\kappa_1}-\frac{\kappa_2}{1+\kappa_2}\right)\right]^{-1}\frac{\Delta cx}{h^2}\Phi(x). \quad (6.3)$$

Conditions of plane strain are again assumed in the solution of eqns (5.27) and (5.28) and for the evaluation of the constants ν_i, κ_i and D^*. Nondimensionalized stresses, loads, moments and rotations are calculated and are transformed back to real quantities through

$$\tau_{zz} = P\bar{\tau}_{zz}/c, \tag{6.4}$$

$$P = \left[\frac{1}{c_{44}}\left(\frac{\kappa_1}{1+\kappa_1} - \frac{\kappa_2}{1+\kappa_2}\right)\right]^{-1}\bar{P}\Delta, \tag{6.5}$$

$$M = \left[\frac{1}{c_{44}}\left(\frac{\kappa_1}{1+\kappa_1} - \frac{\kappa_2}{1+\kappa_2}\right)\right]^{-1}\bar{M}\Delta h, \tag{6.6}$$

$$\theta = \Delta\bar{\theta}/h. \tag{6.7}$$

In order to assess the accuracy of the solution, two tests are performed. First, the rotation of the beam just beyond $x = c$ is compared to that given by the standard beam theory solution:

$$\bar{\theta}_{BT}(\xi) = [P(l_0^2-\varepsilon^2)+2M(l_0+\varepsilon)]/2D^*, \tag{6.8}$$

where $\varepsilon = c^+$. Second, the limit load of the receding contact problem is compared to the beam theory load P_{BT} due to a deflection Δ imposed on a cantilever beam:

$$P_{BT} = 3\Delta D^*/l_0^3. \tag{6.9}$$

The limit load $\lim_{c/h\to 0}\bar{P}_E$ is compared to the value of $\bar{P}_{BT}$ for each case considered.

Once again, if experimental verification of the results is desired, then conditions of plane stress must be assumed in the solution of eqns (5.27) and (5.28) and in the evaluation of displacements and rotations.

7. OBSERVATIONS AND CONCLUSIONS

Beams made of cadmium and magnesium were used in this study as well. For each material, solutions were obtained for $l/h = 10.0, 20.0$, and for each l/h, $l_1/h = 0.25l/h$, $0.5l/h$ and $0.75l/h$. It was found that, except for those beams where the indenter was close to the fixed end and produced a large area of contact, the stress distributions were virtually identical. In those other beams, the stress distributions exhibited a marked increase in the normal stress under the indenter. In these cases, the stress distributions were characterized by a large central bulge, indicating a decline in the antisymmetric component of normal stress. As can be seen in Table 6, these increases in total normal stress can range from 50 to 80% of the normal stress under an indenter that is further away from the fixed end and which produces a smaller contact area. An example of such a stress distribution is given in Fig. 6 for a cadmium beam with $l/h = 20.0$, $l_1/h = 5.0$. Through a comparison with the

Table 6. Total normal stress at origin (Case II; $l/h = 10.0$)

	Cadmium			Magnesium		
c/h	$l_1/h = 2.5$	$l_1/h = 5.0$	$l_1/h = 7.5$	$l_1/h = 2.5$	$l_1/h = 5.0$	$l_1/h = 7.5$
0.2	0.3227	0.3258	0.3191	0.3305	0.3350	0 3126
0.5	0.3907	0.3418	0.3088	0.4173	0.3746	0.2911
0.7	0.4576	0.3411	0.2980	—	0.3931	0.2605
0.9	0.5710	0.3173	0.3023	—	0.2943	0.2905

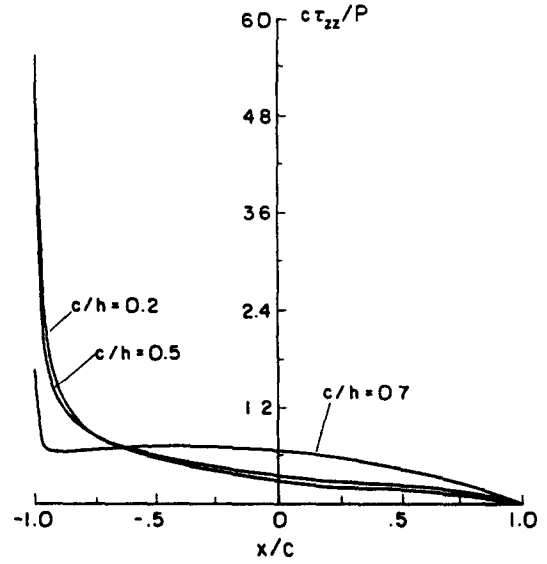

Fig. 6. Total stress distribution (Case II) (cadmium; $l/h = 20.0$, $l_1/h = 5.0$).

normal stresses under an indenter of an isotropic beam [1], it was found that, in cases where the indenter was far away from the fixed end, the stresses in cadmium and magnesium beams were of the same order of magnitude as those in steel beams for cases of small contact, but lower in cases of large contact. Thus the effect of increased anisotropy on the normal contact stress under a flat indenter can vary, depending on the size of the contact area, and on the location of the indenter.

Tables 7 and 9 show a comparison between the elasticity solutions developed here and the corresponding beam theory solutions. The elasticity solutions are seen to agree well with the beam theory solutions. Following the same procedure as before, an upper bound can be placed on the ratio of displacement under the indenter to beam thickness:

$$\Delta/h < \bar{\theta}_0/\bar{\theta}. \tag{7.1}$$

Assuming the value $\bar{\theta}_0 = 0.349$ rad, Table 8 shows the maximum allowable values of Δ/h to ensure small rotations and no yielding.

The phenomena of receding contact is borne out in Table 9 and Fig. 7. As $c/h \to 0$, the nondimensionalized load parameter approaches a limit value greater than zero. In Table 9, the limit loads of the elasticity solutions are seen to agree quite well with the limit loads of the beam theory solutions. An inspection of the limit loads in Table 9 and a comparison with the limit loads for isotropic beams indicates that increased anisotropy results in smaller

Table 7. Rotation comparison (Case II)

		$l_1/h = 2.5$		$l_1/h = 5.0$		$l_1/h = 7.5$		
		Elasticity	Beam theory	Elasticity	Beam theory	Elasticity	Beam theory	c/h
Cadmium	$l/h = 10.0$	0.4791	0.5348	0.2772	0.2848	0.1910	0.1933	0.2
		0.4457	0.4434	0.2612	0.2603	0.1827	0.1823	0.5
		0.4283	0.3843	0.2514	0.2420	0.1775	0.1741	0.7
		—	—	0.2349	0.2092	0.1698	0.1615	1.0
Magnesium	$l/h = 10.0$	0.5192	0.5641	0.2863	0.2922	0.1948	0.1966	0.1
		0.4883	0.5046	0.2745	0.2767	0.1890	0.1896	0.3
		0.4672	0.4484	0.2644	0.2604	0.1833	0.1819	0.5
		—	—	0.2357	0.2069	0.1704	0.1615	1.0

Table 8. Maximum allowable values of Δ/h (Case II)

		$l/h = 10.0$			$l/h = 20.0$		
	c/h	$l_1/h = 2.5$	$l_1/h = 5.0$	$l_1/h = 7.5$	$l_1/h = 5.0$	$l_1/h = 10.0$	$l_1/h = 15.0$
Cadmium	0.2	0.72	1.26	1.85	1.26	2.43	3.57
	0.5	0.78	1.35	1.92	1.33	2.50	3.66
	0.7	0.81	1.38	1.96	1.36	2.56	3.75
	1.0	—	1.49	2.08	—	—	3.84
Magnesium	0.1	0.67	1.21	1.81	1.21	2.38	3.57
	0.3	0.71	1.28	1.85	1.28	2.43	3.66
	0.5	0.75	1.33	1.92	1.31	2.50	3.75
	1.0	—	1.49	2.08	—	—	3.84

Table 9. Limit load comparison (Case II)

		$\lim_{\delta \to 0} \bar{P}_I (\times 10^{-2})$		$\bar{P}_{HT} (\times 10^{-2})$	
	l_1/h	Cadmium	Magnesium	Cadmium	Magnesium
$l/h = 10.0$	2.5	2.2530	2.2400	2.2982	2.2906
	5.0	0.2873	0.2877	0.2874	0.2863
	7.5	0.0850	0.0846	0.0851	0.0848
$l/h = 20.0$	5.0	0.2853	0.2861	0.2874	0.2863
	10.0	0.0355	0.0358	0.0359	0.0358
	15.0	0.0106	0.0106	0.0106	0.0106

limit loads. This agrees with the results for peak total normal stresses under cylindrical indenters.

Upon examination of Fig. 7, it is seen that for the same load, cadmium beams experienced a larger contact area than the corresponding magnesium beams. This behavior is again due to the fact that cadmium beams, being softer in the vertical direction, are penetrated by the indenter, resulting in larger areas of contact. It should be noted that the nondimensionalized load parameter defined in eqn (6.5) has been rewritten as

$$\bar{P} = \lambda_0 h^3 P / D^* \Delta, \tag{7.2}$$

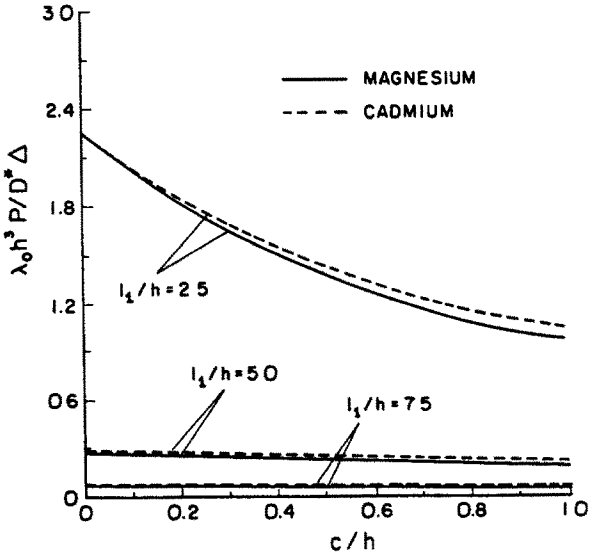

Fig. 7. Load–contact width (Case II) ($l/h = 10.0$)

where λ_0 has the same value as in the case of the cylindrical indenter. Once again, the larger bending stiffness of a cadmium beam increases the area of contact under a flat indenter as compared to the area of contact under the same indenter of the corresponding magnesium beam.

8. SUMMARY

In the present study the behavior of transversely isotropic beams was found to have significantly different results than those of corresponding isotropic beams subjected to similar loadings.

In the case of a cylindrical indenter, it was found that for large contact lengths, highly anisotropic beams exhibited much lower contact stresses than the corresponding isotropic beams. For small contact lengths, the magnitudes of the stresses were relatively equal, and were approximated quite well by Hertzian contact stresses. Furthermore, for a given load, highly anisotropic beams experienced much larger contact areas and much smaller deflections than corresponding isotropic beams. This behavior is due to the fact that in a transversely isotropic beam, the indenter penetrates the material, and as a result produces a larger area of contact and a smaller deflection.

In the case of a flat indenter, it was found that a transversely isotropic beam whose indenter was close to the fixed end and produced a large area of contact experienced a significant increase in total normal stress under the indenter compared with a beam whose indenter was further away from the fixed end. For the cases where the indenter was far from the fixed end, it was found that the normal stress can be larger or smaller than the stress exhibited in isotropic beams, depending on whether the area of contact is small or large, respectively. Furthermore, as in the case of cylindrical identation, for a given load, highly anisotropic beams experienced much larger contact areas.

Lastly, it is noted that the minimum allowable values of R/h and the maximum allowable values of Δ/h are, respectively, less than and greater than their corresponding values for the isotropic beams. This indicates that, for a particular problem configuration, a wider variety of cylindrical and flat indentations may be withstood by transversely isotropic cantilever beams.

Acknowledgement—The authors are grateful for support from the AFOSR (Grant AFOSR-82-0330).

REFERENCES

1. L. M. Keer and W. P. Schonberg, Smooth indentation of an isotropic cantilever beam. *Int. J. Solids Structures* **22**, 87–106 (1986).
2. I. N. Sneddon, *Fourier Transforms*. McGraw-Hill, New York (1951).
3. A. E. Green and W. Zerna, *Theoretical Elasticity*. Oxford University Press, London (1954).
4. L. M. Keer and G. R. Miller, Smooth indentation of a finite layer. *J. Engng Mech. Div. ASCE* **109**, 706–717 (1983).
5. L. M. Keer and R. Ballarini, Smooth contact between a rigid indenter and an initially stressed orthotropic beam. *AIAA J.* **21**, 1035–1042 (1983)